POSSIBLE PRECESSION MOTION IN THE BIPOLAR PROTO-PLANETARY NEBULA IRAS 17441−2411

Kevin Volk

Gemini Observatory, Hilo, Hawaii

kvolk@gemini.edu

and

Sun Kwok

University of Hong Kong, Hong Kong, China
and
Department of Physics and Astronomy, University of Calgary, Calgary, AB T2N 1N4, Canada

sunkwok@hku.hk

ABSTRACT

Mid-infrared imaging of two bipolar proto-planetary nebulae IRAS 17150−3224 and IRAS 17441−2411 were obtained at the Gemini Telescope. Dust emissions are detected in both the bipolar lobes and in the equatorial region of IRAS 17441−2411. In particular, the orientation of the axis of the infrared torus is found to be offset by 23° from the bipolar axis. If the torus is responsible for or related to the collimation of the bipolar outflow, this raises the possibility that the outflow has undergone precession over the last 100 years.

Subject headings: circumstellar matter: — infrared: stars —- planetary nebulae: general — stars: AGB and post-AGB

1. Introduction

IRAS 17150−3224 (AFGL 6815S, the "Cotton Candy Nebula") and IRAS 17441−2411 (or AFGL 5385, the "Silkworm Nebula") were first identified as a bipolar proto-planetary nebula (PPN) as the result of an imaging survey of cool IRAS sources (Kwok et al. 1996). Subsequent *Hubble Space Telescope (HST)* observations have shown that each object consists

of a pair of bipolar reflection nebulae separated by a dark dust lane (Kwok et al. 1998; Su et al. 1998). These two objects are often cited as prime examples to support the thesis that the bipolar morphology of PN develops early, shortly after the end of the asymptotic giant branch (AGB) and before the onset of photoionization. Of particular interest is the possible role of the equatorial torus, whose existence is implied by the dark lane, in the collimation of a fast outflow that shape the morphology of the nebula.

A variety of scenarios have been proposed to explain the transformation of the spherical circumstellar envelopes of AGB stars into a bipolar morphology seen in many planetary nebulae (PN) (Balick & Franck 2002). Most of the theories involve the development of a post-AGB fast, collimated outflow that carves out bipolar cones from the pre-existing spherical circumstellar envelope of the AGB star. The lower density of the cavity allows the scattered light from the central star to escape, leading to the optical illuminatiion of the reflection bipolar nebulosity. The physical mechanism of the fast outflow, in particular, the collimation mechanism, remains unidentified. Some theories, e.g., those involving magnetic fields or binary central stars, include a circumstellar disk/torus as a means of collimation (García-Segura et al. 1999; Soker & Rappaport 2000). Specifically, the effects of a low-mass companion in creating a disk-driven jet through different scenarios of common-envelope evolution are explored by Nordaus & Blackman (2006). It is clear that these models can only be tested with the direct observations of such disks or torus.

Since the disk/torus is likely to be of high density and made up of dust and molecular gas, it can only be directly imaged in the mid-infrared or in the submillimeter regions. Given the small sizes of PPNs, imaging capability of very high resolution is required. In the submillimeter, it can be achieved by submm interferometers such as *PdBI, CARMA, SMA*, and *ALMA*, and in the mid-infrared, by ground-based telescopes of large aperture equipped with adaptive optics capabilities. We have carried out a survey of a number of PPNs and PNs using Gemini North and South 8 m Telescopes. In this paper, we report the new results on the infrared imaging of two PPNs.

2. Observation

Mid-infrared imaging observations of IRAS 17150−3224 and IRAS 17441−2411 were made under program GS-2004A-Q-56 on the nights of 23 June 2004 and 6 July 2004, with the Thermal Region Camera Spectrograph (T-ReCS). T-ReCS is the facility mid-infrared imager and long-slit spectrograph at Gemini South built by the University of Florida. It employs a Raytheon Si:As Impurity-band Conductor (IBC) array having a 320×240 pixel format with pixel scale of $0\farcs09$ and a field of view of $28\farcs8 \times 21\farcs6$. The instrument design is

optimized for low thermal background, high throughput, and excellent image quality in the mid-infrared wavelength region between 8 to 26 μm to take advantage of the high thermal-infrared performance of the Gemini telescopes. T-ReCS, combined with Gemini's fast tip/tilt compensating secondary mirror, yields nearly diffraction-limited images under most natural seeing conditions. The diffraction-limited spatial resolution of T-ReCS at 10 μm is $\sim$0$''$.35.

Imaging observations were carried out with medium-band filters at N and Q bands: namely, Si-2 (central wavelength $\lambda_0 = 8.8$ μm; bandwidth $\Delta\lambda = 0.72$ μm); Si-5 ($\lambda_0 = 11.66$ μm, $\Delta\lambda = 1.13$ μm); and Qa ($\lambda_0 = 18.30$ μm, $\Delta\lambda = 1.51$ μm). IRAS 17150−3224 was observed with the Si-2 and Qa filters while IRAS 17441−2411 was observed with the Si-2 and Si-5 filters. For each object standard star observations were made for the same filters to determine the point spread function (PSF) as well as for flux calibration. The standard stars used are HD 169916 and HD 175775 for IRAS 17150−3224 and IRAS 17441−2411, respectively.

Accurate cancellation of the mid-infrared sky and telescope background radiation was obtained by the technique of chopping and nodding. The secondary mirror is capable of 2-point (square wave) chopping at an arbitrary position angle on the sky, with the chop frequency of 3 Hz and an amplitude of $\pm$ 7$''$.5 (the maximum chopper throw is 15$''$, which is considerably smaller than the T-ReCS field of view). T-ReCS observations were taken in ABABABAB nodding pattern. The data were created in the multiple extension FITS (MEF) format with one extension for one NOD position. Multiple frames taken with each frame integration time of 34.47 ms for the Si-2 observations and 25.86 ms for the Si-5 and Qa observations. The MEF frames were stacked and reduced with the standard pipeline reduction task *mireduce* in gemini package of IRAF. The reduced data were then subjected to the photometric calibration using the standard star observations. For this purpose the absolute fluxes of the calibration stars were taken from Cohen et al. (1999). The fluxes were integrated over the filter profile and weighted by photon number to produce the expected in-band fluxes in the different filters.

The reduced T-ReCS images were then deconvolved using the PSF image of their respective filters. We have adopted *Lucy* deconvolution algorithm available in IRAF and the deconvolved images were then smoothed with a 2×2 matrix to improve the S/N ratio. The final spatial resolution for these images is 0$''$.18.

3. Results

Figure 1 shows the Gemini Si-2 and Qa band images of IRAS 17150−3224. The dust emission is located at the position of the central star. From the *ISO* spectra of these two objects (Fig. 2), their infrared emissions are dominated by a dust component of temperature of ∼150 K and therefore are expected to be brighter in the Q band than in the N band. The image is basically unresolved in the N band, and marginally resolved in Q band.

Figure 3 shows the Si-2 and Si-5 images of IRAS 17441−2411. A double-peak structure, which can be interpreted as an edge-on torus, can clearly be seen. Dust emission is also observed in the bipolar lobes, which appear to be closed at the ends. However, when one examines the fainter level of emissions, a "S-shape" point-symmetric structure can clearly be seen, in particular in the Si-5 image. The orientation of the equatorial torus and the infrared lobes can be compared to the orientation of the dark lane and reflection nebulosities in the optical (Fig. 4). The plane of the torus can be determined by drawing a line across the two central infrared peaks, which is shown as a solid line in left panel of Fig. 4. We have overlaid the orientation of the torus on the *HST* I-band image of IRAS 17441−2411 (right panel of Fig. 4). It is clear that the orientation of the infrared disk is not perpendicular to the optical bipolar lobes. The angular separation between the infrared disk and the dark lane in the optical image is estimated to be 23°.

Since standard stars were observed, we are able to derive the total fluxes in the filters observed. For IRAS 17441−2411, the fluxes in the Si-2 and Si-5 filters are 12.75± 0.05 and 39.1± 0.16 Jy, respectively (not corrected for differential atmospheric extinction between the objects and the standard stars). These can be compared to the fluxes estimated from the *IRAS Low Resolution Spectra (LRS)* and *Infrared Space Observatory (ISO)* observations at their respective central wavelengths. The simulated *LRS* and *ISO* fluxes are obtained by first calibrating the spectra by the *IRAS Point Source Catalog* 12 μm fluxes, and then integrated over the T-ReCS filters. For the Si-2 filter, the simulated fluxes are 12.80 Jy (*LRS*) and 9.35 Jy (*ISO*), and for the Si-5 filter, 36.7 (*LRS*) and 31.54 (*ISO*) Jy. It is unclear why the fluxes from the *IRAS* and *ISO* observations should differ from each other, as the source is small and should lie well within the *ISO* aperture. It is also unlikely that the flux should have varied over the period between the *IRAS* and *ISO* observations.

For IRAS 17150−3224, the T-ReCS fluxes at Si-5 filter is 44.82±0.30 Jy, compared to the simulated *ISO* flux of 41.61 Jy. At the Qa filter, the T-ReCS flux is 184.3±4.0 Jy, compared to the simulated *ISO* flux of 200.6 Jy.

In our experience, the winter weather in Pachon is generally poorer for mid-IR observations than in the summer or fall. Under the best weather stable conditions, photometric

accuracy of 1-2% is possible. Since our data were taken in late June/early July, the accuracy of the photometric measurements is not expected to be better than 6-8%. With changing water vapor content, the error at the Q band can be higher. There is therefore reasonable agreements between the T-ReCS and *IRAS LRS* observations.

4. Discussion

4.1. A precessing outflow?

While the existence of dark lanes in the optical images of galaxies or star formation regions are usually interpreted as evidence for the existence of a dusty torus, direct infrared imaging on IRAS 17441−2411 for the first time opens the possibility that this relationship is not necessarily a simple one. Since the nebulae are optically thin in the mid-infrared, the intensity in the infrared images should directly trace the density distribution of dust. It should be noted, however, that the optical nebulosity traces the scattered light reflected off the cavity carved out of the remnant spherical AGB envelope by the high-velocity outflow. The fact that the bipolar flow did not emerge perpendicularly from the torus is an unexpected outcome of the present observations. Such a misalignment between the outflow direction and the axis of the torus may be related to the phenomenon of multiple bipolar lobes in PN, examples of which include NGC 2440 (López et al. 1998), Hen 2-47 and M1-37 (Sahai 2000), and NGC 6881 (Kwok & Su 2005). Although the origin of multiple lobes is not known, precession has been suggested to be one of the possible causes (Miranda et al. 1999). Direct evidence of the precession of a magnetically collimated jet has been observed in W43A (Vlemmings et al. 2006) and we have to seriously consider precessing outflows as a common phenomena in PPNs and PNs.

Independent evidence for precession can also be found in the near infrared image of IRAS 17441−2411. In the *HST* NICMOS F160W and F222M images, the bipolar lobes show a point-symmetric S-shape, with the ends of the lobes pointing away from N-S directions to NW-SE directions (Fig. 4a and 4b, Su et al. 2003). In fact, the S-shape structure of the bipolar lobes can also be seen in dust emission in Figure 3. We note that at present, the axis of the torus is along the NE-SW directions and the main lobes are approximately aligned along the NNE-SSW directions. The tips of the S-shape structure seen in the fainter emissions, however, point to the NW-SE directions. If we interpret these different orientations as the result of the nebula having undergone precession motion, then the torus must have rotated by almost 90° in the recent past. The approximate interval of this precessing motion can be roughly estimated as follows. From the *HST* WFPC2 image of IRAS 17441−2411, the lobes have angular sizes θ of approximately $2''$ (Su et al. 1998). For an assumed distance

D of 1 kpc and a fast outflow velocity of 100 km s^{-1}, the kinematic age of the lobes is $\sim (\theta/2'')(D/\mathrm{kpc})(V/100\ \mathrm{km/s})^{-1} \sim 100$ yr. If the misalignment is indeed due to precession, then the torus must have precessed at a rate of approximately 1° per yr. If the precession is caused by a binary central system or magnetic fields, then this kinematic age can be used to infer the orbital period, central masses and separations, or the magnetic field strengths (García-Segura 1997). For example, this large precession rate may pose a problem for the magnetic driven model.

4.2. An accretion disk?

The infrared torus observed in Fig. 3 is large ($\sim$ 1000 AU), and therefore unlikely to be the primary agent that drives the precession. Instead, the infrared torus could be created in response to the precessing outflow, which is driven by a much smaller, central precessing disk. For example, if the outflow has a modest opening angle, the torus could represent circumstellar material accumulated in the equatorial directions due to the absence of outflow there. If the central precessing disk is caused by a binary system, the the central disk could be an accretion disk.

We therefore have the following model for IRAS 17441−2411. A spherical dust envelope is created by a slow wind from an AGB star. As the AGB star evolves and gets larger, its stellar wind is gradually accreted by a secondary companion main-sequence star, resulting in an accretion disk. A collimated high-velocity outflow emerges perpendicular to the disk (Soker & Livio 1994). This fast outflow sweeps away the circumstellar material and creates a cone-like cavity. The cavity is seen as reflection nebula as star light is reflected off the walls of the cavity. Circumstellar dust in the equatorial directions is seen as an infrared torus. Due to orbtal motion or other reasons, the accretion disk begins to precess. The changing directions of the outflow sweeps out a cavity into a "S" shape and the orientation of the infrared torus responds in changing its own orientation.

The feasibility of the accretion model can also be constrained by the observed mechanical power in the fast outflow. Since the visual brightness of PPNs are due to scattered starlight and not due to emission lines as in the case of PNs, we have no kinematic information on the outflows. However, the detection of shock-excited H_2 emission can be used to produce some observational constraints. From the H_2 spectra of IRAS 17150−3224, Hrivnak et al. (2006) estimate a shock velocity of $\sim$40 km s^{-1}. The mass of the fast outflow is uncertain as the observed emissions originates from clumps at the end of the lobes, which is likely to consist mostly of swept-up gas. If we assume a mass loss rate of 10^{-7} M$_\odot$ yr^{-1} for the fast outflow, the corresponding mechanical luminosity is $\sim 5 \times 10^{31}$ erg s^{-1}. If we assume 0.1%

of a stellar wind of mass loss rate 10^{-5} $M_\odot$ yr^{-1} is accreted onto a 0.3 $M_\odot$ main-sequence secondary star, the corresponding accretion power is $\sim 10^{33}$ erg s^{-1}, which is small compared to the luminosity of the AGB star but is still larger than the estimated mechanical energy of the fast outflow. Due to the uncertain observational and theoretical parameters, the test cannot be considered as conclusive.

In a recent paper, Huggins (2007) suggests that such an accretion-ejection sequence can be tested by observing the dynamical ages of the tori and jets. Since the jet formation is governed by the thermal time scale of secondary, the time scale is longer than the observed lag time of a few hundred years in the sample studied by Huggins (2007). In any case, the fact that the tori of PNs and PPNs can be observed in high angular resolution in the mid-IR and submm opens the possibility that ejection mechanisms can be quantitatively tested and therefore represents a potentially powerful tool to discriminate between models.

4.3. Geometry and chemical composition of the torus

We can also obtain some information on the infrared torus from the spectra. From the *ISO* spectra of the two objects (Figure 2), we can see that IRAS 17150−3224 has a smooth dust continuum with the exception of a silicate absorption feature at 9.7 μm. We should note that the detection of a silicate absorption feature in a post-AGB star is very unusual. This is probably the result of viewing the torus edge on, leading to a larger optical depth in the line of sight.

For IRAS 17441−2411, a strong, broad emission feature between 23.5 and 28 μm can be seen in its *ISO* spectrum. This feature is similar to the 30 μm feature commonly observed in PNs and PPNs (Volk et al. 2002). The broad plateau emission feature in the 12-17.5 μm region also resembles features seen in carbon-rich PPNs (Hrivnak et al. 2000). Although these two broad features suggest a carbon-rich nature of the object, the 3.3, 6.2, 7.7, and 11.3 μm aromatic infrared bands (AIB) are not seen. When viewed in the evolutionary scenario outlined in Volk et al. (2002) and Kwok (2004), the absence of AIB features can be understood by the suggestion that IRAS 17441−2411 is in such an early stage of post-AGB evolution that the aromatic components are still in small units with many aliphatic side groups. It is only later in the evolution that the aromatic rings are grouped in larger clusters (Kwok et al. 2001).

5. Conclusions

The physical mechanism responsible for the launching of bipolar outflows in young and evolved stars continues to be a major unresolved problem in astrophysics. The high-angular resolution capabilities in the mid-IR can now measure the size and orientation of the central tori of PNs and PPNs. These measurements have the potential of quantitatively testing the models of how the fast outflows ("jets") are launched from the tori. In addition, the observation of multipolar nebulosities in PNs raises new questions on time variability of the launch angle. The observations presented here provide for the first time a direct quantitative measure of the angle between the disk and the bipolar outflow. In the case of IRAS 17441−2411, there is evidence that the disk has precessed on a time scale of 10^2 yr. If these values are supported by further observations in other objects, then they represent strong constraints on the physics at work in the central engines of bipolar nebulae.

Acknowledgments

We thank Noam Soker for his valuable comments on the manuscript. This work is based on observations obtained at the Gemini Observatory, which is operated by the Association of Universities for Research in Astronomy, Inc., under a cooperative agreement with the NSF on behalf of the Gemini partnership: the National Science Foundation (United States), the Particle Physics and Astronomy Research Council (United Kingdom), the National Research Council (Canada), CONICYT (Chile), the Australian Research Council (Australia), CNPq (Brazil) and CONICET (Argentina). SK acknowledges support of this research by the Research Grants Council of Hong Kong and by the Natural Sciences and Engineering Research Council of Canada.

REFERENCES

Balick, B., & Frank, A. 2002, ARAA, 40, 439

Cohen, M., Walker, R.S., Carter, B. et al. 1999, AJ, 117, 1864

García-Segura, G. 1997, ApJ, 489, L189

García-Segura, G., Langer, N., Rózyczka, M., & Franco, J. 1999, ApJ, 527, 767

Hrivnak, B.J., Volk, K., & Kwok, S. 2000, ApJ, 535, 275

Hrivnak, B.J., Kelly, D.M., Su, K.Y.L., Kwok, S., & Sahai, R. 2006, ApJ, 650, 237

Huggins, P.J. 2007, ApJ, 663, 342

Kwok, S. 2004, Nature, 436, 985

Kwok,S., and Su, K.Y.L. 2005, ApJ, 635, L49

Kwok, S., Hrivnak, B.J., Zhang, C.Y., Langill, P.L. 1996, ApJ, 472, 287

Kwok, S., Su, K.Y.L., & Hrivnak, B.J. 1998, ApJ, 501, L117

Kwok, S., Volk K., & Bernath, P. 2001, ApJ, 554, L87

López, J.A., Meaburn, J., Bryce, M., Holloway, A.J. 1998, ApJ, 493, 803

Miranda, L.F., Guerrero, M., Torrelles, J.M. 1999, AJ, 117, 1421

Nordhaus J., Blackman E. G., 2006, MNRAS, 370, 2004

Sahai, R. 2000, ApJ, 537, L43

Soker, N., & Livio, M. 1994, ApJ, 421, 219

Soker, N., & Rappaport, S. 2000, ApJ, 538, 241

Su, K.Y.L., Volk, K., Kwok, S., & Hrivnak, B.J. 1998, ApJ, 508, 744

Su, K.Y.L., Hrivnak, B.J., Kwok, S., & Sahai, R. 2003, AJ, 126, 848

Vlemmings, W.H.T., Diamond, P.J., & Imai, H. 2006, Nature, 440, 68

Volk, K., Kwok, S., Hrivnak, B.J., Szczerba, R. 2002, ApJ, 567, 412

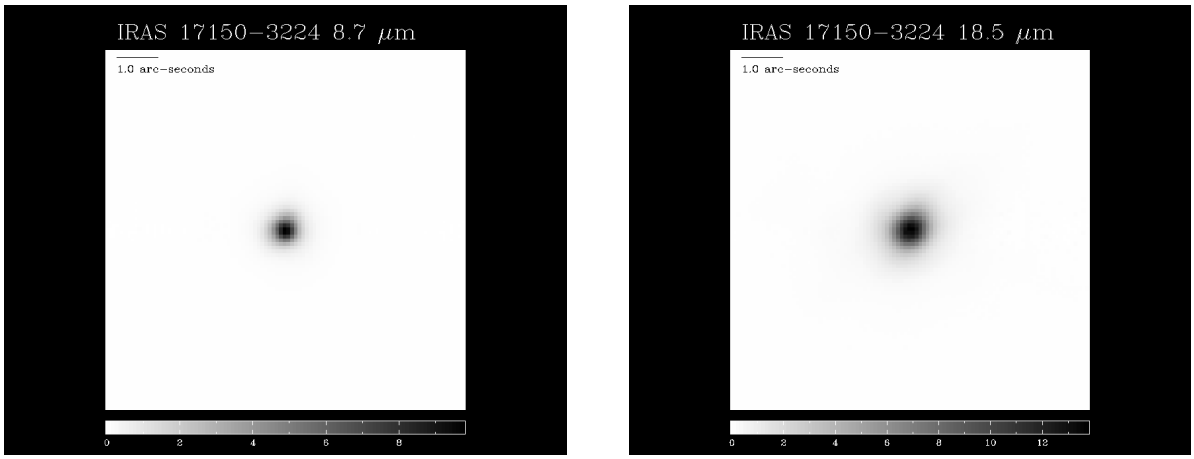

Fig. 1.— Gemini T-ReCs Si-2 (left) and Qa (right) images of PPN IRAS 17150−3224 after deconvolution. The Gemini image is on a linear scale with the grey scale in units of Jy/sq. arc sec. North is up and East is to the left.

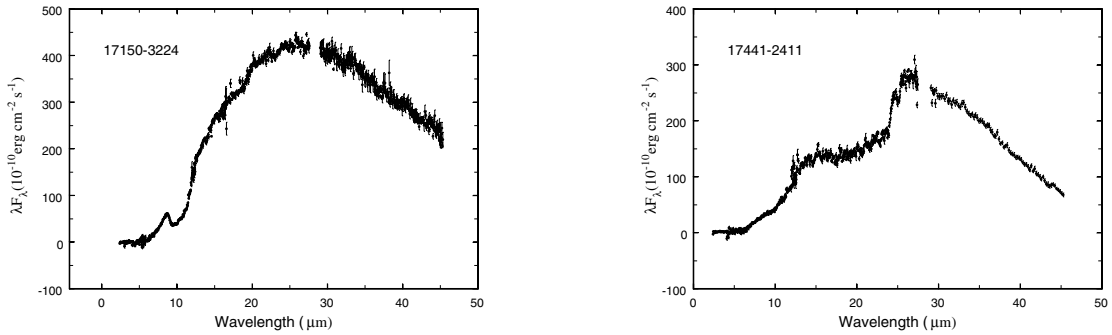

Fig. 2.— ISO SWS01 spectra of IRAS 17150−3224 (left) and IRAS 17441−2411 (right). The spectra of IRAS 17150−3224 and IRAS 17441−2411 were obtained in the ISO guest observing programs SWSPPN01 (PI: B.J. Hrivnak) and LOWTEMPL (PI: K. Volk), respectively, and the data were processed by KV. The data between 27.0 and 29.0 μm are omitted due to problems with the ISO band 3E detector.

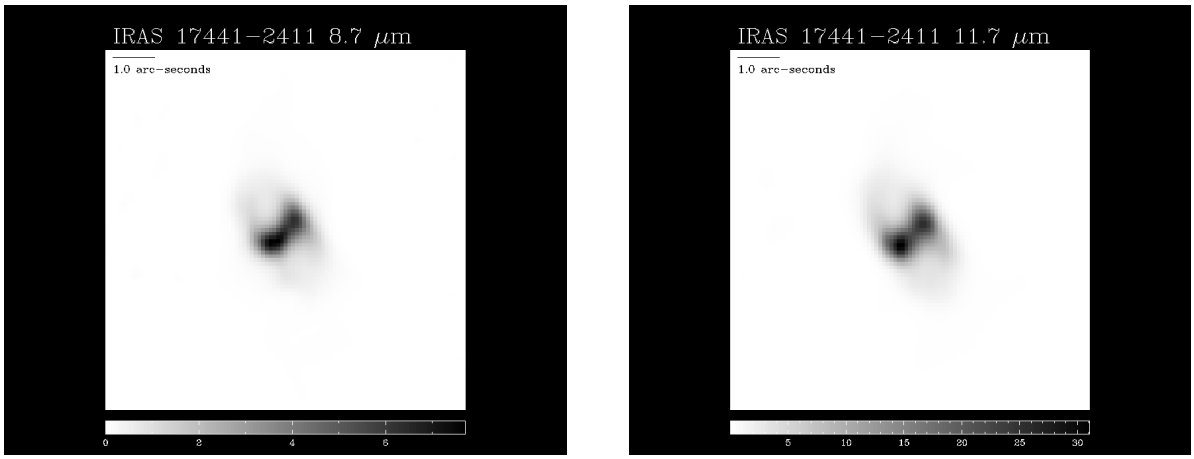

Fig. 3.— Gemini T-ReCs Si-2 (left) and Si-5 (right) images of PPN IRAS 17441−2411 after deconvolution. The Gemini image is on a linear scale with the grey scale in units of Jy/sq. arc sec. North is up and East is to the left.

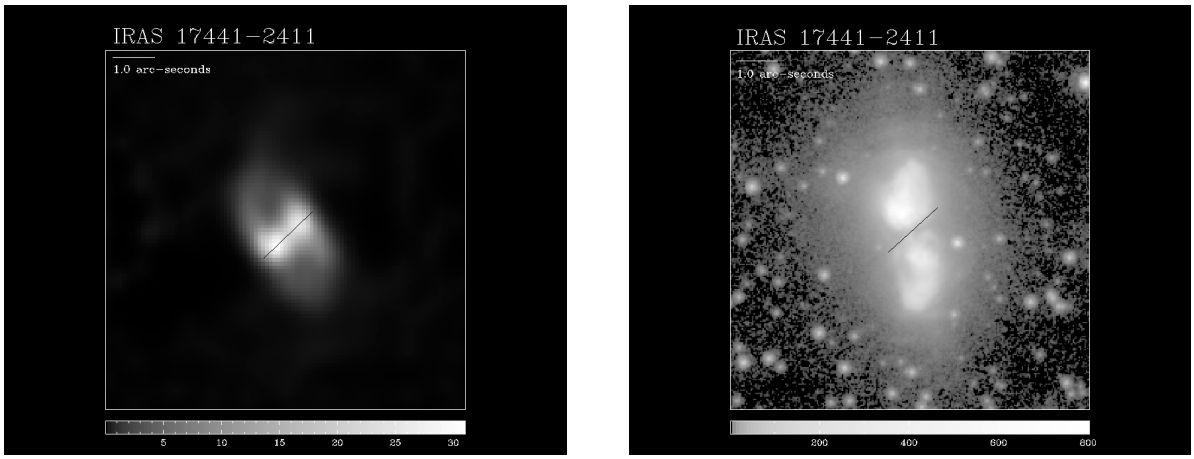

Fig. 4.— Gemini T-ReCs 11.7 μm images of PPN IRAS 17441−2411 (left). The orientation of the infrared disk is overlaid on the optical I band *HST* image (right) as a solid line. The Gemini image is on a linear scale with the grey scale in units of Jy/sq. arc sec. The *HST* image is in logarithmic units of raw counts. North is up and East is to the left.